Research Article

Ahmed A. H. Abdellatif*, Riaz A. Khan, Ahmad H. Alhowail, Abdulmajeed Alqasoumi, Sultan M. Sajid, Ahmed M. Mohammed, Mansour Alsharidah, Osamah Al Rugaie, and Ayman M. Mousa

Octreotide-conjugated silver nanoparticles for active targeting of somatostatin receptors and their application in a nebulized rat model

Abstract: Drug uptake and distribution through cell–receptor interactions are of prime interest in reducing the adverse effects and increasing the therapeutic effectiveness of delivered formulations. This study aimed to formulate silver nanoparticles (AgNPs) conjugated to somatostatin analogs for specific delivery through somatostatin receptors (SSTRs) expressed on cells and by nebulizing the prepared AgNPs formulations into lung cells for *in vivo* application. AgNPs were prepared using the citrate reduction method, yielding AgNPs–CTT, which was further chemically conjugated to octreotide (OCT) to form AgNPs–OCT through an amide linkage. The AgNPs–OCT formulation was coated using alginate to yield a carrier, AgNPs–OCT–Alg, feasible for drug delivery through nebulization. AgNPs were uniform in size with an acceptable range of zeta potential. Furthermore, the concentrations of AgNP formulations were found safe for the model cell lines used, and cell proliferation was significantly reduced in a dose-dependent manner ($p < 0.05$). In the healthy lung tissues, AgNPs–OCT–Alg accumulated at a concentration of 0.416 ± 5.7 mg/kg$_{\text{tissue}}$, as determined *via* inductively coupled plasma optical emission spectrometry. This study established the accumulation of AgNPs, specifically the AgNPs–OCT–Alg, in lung tissues, and substantiated the active, specific, and selective targeting of SSTRs at pulmonary sites. The anticancer efficacy of the formulations was *in vitro* tested and confirmed in the MCF-7 cell lines. Owing to the delivery suitability and cytotoxic effects of the AgNPs–OCT–Alg formulation, it is a potential drug delivery formulation for lung cancer therapy in the future.

Keywords: silver nanoparticle, somatostatin receptor, active targeting, octreotide, *in vivo* lung cancer delivery, molecular modeling, receptor binding

* **Corresponding author: Ahmed A. H. Abdellatif,** Department of Pharmaceutics, College of Pharmacy, Qassim University, Qassim 51452, Saudi Arabia; Department of Pharmaceutics and Pharmaceutical Technology, Faculty of Pharmacy, Al-Azhar University, Assiut 71524, Egypt, e-mail: a.abdellatif@qu.edu.sa
Riaz A. Khan: Department of Medicinal Chemistry and Pharmacognosy, College of Pharmacy, Qassim University, Qassim 51452, Saudi Arabia
Ahmad H. Alhowail, Sultan M. Sajid: Department of Pharmacology and Toxicology, College of Pharmacy, Qassim University, Qassim 51452, Saudi Arabia
Abdulmajeed Alqasoumi: Department of Pharmacy Practice, College of Pharmacy, Qassim University, Qassim 51452, Saudi Arabia
Ahmed M. Mohammed: Department of Pharmaceutics and Pharmaceutical Technology, Faculty of Pharmacy, Al-Azhar University, Assiut 71524, Egypt
Mansour Alsharidah: Department of Physiology, College of Medicine, Qassim University, Buraydah 51452, Saudi Arabia
Osamah Al Rugaie: Department of Basic Medical Sciences, College of Medicine and Medical Sciences, Qassim University, Unaizah, P.O. Box 991, Al Qassim 51911, Saudi Arabia
Ayman M. Mousa: Department of Basic Health Sciences, College of Applied Medical Sciences, Qassim University, Qassim 51452, Saudi Arabia; Department of Histology and Cell Biology, Faculty of Medicine, Benha University, Benha, Egypt

1 Introduction

It is difficult to diagnose lung cancer because it has no early observable symptoms. Thus, the tumor is typically advanced at the time of primary diagnosis and continues to progress [1,2]. Currently, although radiotherapeutic and chemotherapeutic interventions are available as part of lung cancer treatment modalities, their harmful effects on normal and other noncancerous cells have limited their role, and research has been conducted to determine alternative treatment approaches [3]. These limitations and applications to treatment, through radio-oncologic modalities, have also led to dose perturbations with uncertain modulations during drug and radiological dose delivery.

However, the side effects of these treatment modalities have not yet rendered them ineffective; therefore, even with putative damage to normal or non-cancerous cells, studies on improving the efficacy and drug- and radiation-dose controls are under development. Although the effectiveness of a drug increases as its dose increases, the increase in the dose is limited by the inherent toxicity of the drug and the radio-intervention, leading to undesired physiological and morphological changes and the destruction of normal cells [4]. The inhalation route of drug delivery is considered an effective strategy for the treatment of lung diseases [5]. This route of drug administration shows favorable advantages in targeted organs such as the lungs because the drug can reach the sites directly through inhalation, provided that the carrier-based formulation and the drug to be delivered are feasible for inhalation. Both show receptivity to diseased tissue parts. In this case, the direct delivery of the drug to the lungs has the advantage of lowering the required dose of the drug, which would otherwise have been higher and required more frequent administrations. It also specifically targets cancer sites and reduces the toxic effects on normal/non-cancerous lung cells, which is feasible [6].

Breast cancer is the commonest cancer among women and the leading cause of cancer-related deaths worldwide. Breast cancer is initiated when the cells of the breast undergo uncontrolled division. Symptoms of breast disease include breast masses, changes in the volume of the breast, breast discomfort, and nipple discharge. A hard, painless mass in one of the nipples is the most common symptom of breast disease in males [7]. Currently, available treatment modalities for breast cancer include radiotherapy and chemotherapy; however, radiotherapy damages normal cells in addition to cancer cells. Chemotherapy can also be administered after surgery and radiotherapy [3]. However, cancer chemotherapy is limited due to its toxicity to normal cells. Moreover, increasing the dose can increase the effectiveness of chemotherapy [4]. However, many new drugs result in severe forms of toxicity, mainly in the form of myelo-suppression [8]. Delivering cytotoxic agents directly to tumor cells is more beneficial in terms of dose increase, reduction in the occurrence of peripheral toxicity, and improvement of therapeutic efficiency. Active targeting is considered an effective strategy for curing breast cancer. Further, there is a need to reduce the systemic side effects of parenteral and oral chemotherapy by using site-specific formulas.

Silver nanoparticles (AgNPs) are considered one of the most promising nanostructures. Their favorable physico-chemical characteristics and bioactive properties have been found to be appropriate for several biomedical applications in vitro and in vivo. Intense interest in AgNPs and their derivatives has improved the treatment choices for currently available oncological interventions [9]. AgNPs have many applications in the medical, biomedical, and biotechnical fields, including cancer cell targeting therapy, and several other biomedical treatment arenas [10]. Although all studied AgNPs were previously formulated only for inhalation as a passive targeting strategy or to determine their cytotoxicity [11–13], AgNPs can be applied in active targeting via receptors. Moreover, ligand-coated AgNPs can target specific receptors in the human body, such as somatostatin (SST) receptors (SSTRs), which are among the most abundant receptors expressed by lung tumor cells [14]. High- and low-affinity SSTRs have been identified in numerous cancer cells, such as those of the lung, ovaries, pancreas, colorectum, and prostate [15,16]. Furthermore, SST analogs, such as octreotide (OCT) and vapreotide (VAP), have also been shown to have high and specific affinities to SSTR subtypes 2 and 5 [17,18]. OCT binds directly to receptors on tumor cells, as a majority of human tumor cells, either benign or malignant, usually express SSTRs [19]. Nilsson et al. have reported that numerous normal and infected human cells overexpress SSTRs. This makes SSTRs (particularly, $SSTR_2$) feasible and promising target ligands using OCT or VAP-conjugated nanoparticulate delivery systems to reduce side effects and increase the accumulation of drugs in tumor cells [20]. Dasgupta et al. confirmed the delivery of OCT to cancer cells that express SSTRs, while Norenberg et al. reported that SST analogs widely used to target cancer cells express SSTRs for therapy with ^{90}Y or ^{177}Lu radionuclides [21].

Currently, no studies have reported the use of an AgNPs-conjugated SST analog OCT to target lung cancer via inhalation. This study aimed to develop a simple, non-invasive, aerosol-based, site-specific method to deliver a payload (drug) to the lung tissues for delivery by nebulization for in vivo inhalation and subsequently targeted delivery.

2 Methods

2.1 Materials

Silver nitrate ($AgNO_3$), tri-sodium citrate (TSC), sodium alginate (Alg), sodium chloride, potassium chloride, potassium dihydrogen phosphate, sodium hydroxide, and disodium hydrogen phosphate were purchased from El Nasr Pharmaceuticals Chemicals Company (Abu Zaabal, Cairo,

Egypt). OCT acetate, Gibco Roswell Park Memorial Institute (RPMI) 1640 medium with 10% fetal bovine serum (FBS), and antibodies were purchased from Santa Cruz Biotechnology Inc. (Heidelberg, Germany). The tumor necrosis factor (TNF)-α inhibitor was purchased from Calbiochem (San Diego, CA, USA). Kits for cytokine-specific enzyme-linked immunosorbent assays (ELISAs) were purchased from R&D Systems, Inc. (St. Paul, MN, USA). The Michigan Cancer Foundation-7 (MCF-7) cell line was obtained from Vacsera (Dokki, Giza, Egypt). All chemicals were of analytical grade.

2.2 Synthesis of silver citrate nanoparticles by the reduction technique

Citrate-reduced and capped AgNPs (AgNPs–CTT) were prepared using the citrate reduction method following a previously reported protocol [22] with some modifications using 100 mL of aqueous $AgNO_3$ (molecular weight, 169.87; 0.05 mol; 8.4935 g) solution. Briefly, 28 mg of $AgNO_3$ was diluted in 50 mL of Millipore-purified water (stock solution I). The stock solution I (6.5 mL) was diluted to 100 mL with Millipore water. The solution was stirred vigorously at 6,000 rpm to 100°C. About 2 mL of 2% TSC solution was slowly and carefully added to the boiling $AgNO_3$ solution in an Erlenmeyer flask and allowed to continue boiling for 15 min. The colorless solution changed to yellow, bright red, red, and brown, indicating completion of the reaction after 15 min. The AgNPs–CTTs were stored at room temperature (27°C) in amber-colored bottles. The particles were purified by centrifugation at 1,200 rpm for 6 min to remove large particulate matter.

2.3 Preparation of AgNPs–CTT capped with OCT and wrapped with alginate

The OCT was selectively conjugated to AgNPs–CTT through its N-terminus [23]. The AgNPs–CTT formed at a concentration of 0.1 mM was reacted with a two-fold excess of OCT. Then, 100 μL of 0.2 mM OCT was added to the reaction mixture, followed by the addition of 0.15 mM *N*-(3-dimethylaminopropyl)-*N'*-ethyl carbodiimide hydrochloride (EDC) and 0.2 mM *N*-hydroxysuccinimide, and stirred for an additional 3 h at room temperature. The final product, AgNPs–OCT, was purified by centrifugation at 1,200 rpm for 5 min to remove large particulate matter [24]. The AgNPs–OCT formulation was optimized for lung delivery by stirring

AgNPs through dispersion in a sodium alginate aqueous solution (1%), which generated a coat of alginate around the AgNPs–OCT. The formulated AgNPs–OCT–Alg was prepared to enhance AgNPs–OCT delivery into the lungs through inhalation.

We calculated the amount of Ag^+ transformed to Ag^0, which represents the percent yield of the produced AgNPs, using the previously described approach with some minor modifications [25,26]. Inductively coupled plasma optical emission spectrometry (JY-70 PLUS, Jobin Yvon Instruments SA Inc., Edison, NJ, USA) was used to calculate the amount of Ag^0 in all AgNP formulas. Each formula was centrifuged at 1,200 rpm for 5 min in order to separate the large particulate and remove the impurities. The supernatant was evaluated by ICP-OES. The quantity of silver Ag^0 was measured in the supernatant and then divided by the initial concentration of $AgNO_3$. 5 Each solution was scanned times. The % yield of the produced AgNPs was calculated by dividing the obtained concentration by the initial concentration for $AgNO_3$ using the following equation:

$$\% \text{ AgNPs yield} = \left[\frac{\text{Concentration of each sample by ICP OES}}{\text{Initial concentration of AgNO}_3} \right] \times 100. \quad (1)$$

2.4 Size and zeta potential measurements

A Malvern Zetasizer Nano 6.01 analyzer (Malvern Instruments GmbH, Herrenberg, Germany) was used to measure the particle size, polydispersity index, and zeta (ζ) potential. Sampling times were automatically set on the instrument. Three measurements were permitted for every 10 subruns. All calculations were performed according to previously described protocols [14,27].

2.5 UV-Vis spectroscopy

The absorption spectra of AgNPs–CTT, AgNPs–OCT, and AgNPs–OCT–Alg formulations were recorded. The absorption spectrum for each formulation was scanned in the range of 300–700 nm in a 2/cm plastic cuvette using the Uvikon-941 spectrophotometer (Kontron Device GmbH, Herrenberg, Germany). Surface plasmon resonance (SPR) peaks were obtained using Microsoft Excel for Macintosh 2019 (Microsoft Corporation, Redmond, WA, USA) [14].

2.6 Cell culture

2.6.1 Toxicity study

MCF-7 cells were grown in the Gibco RPMI 1640 medium containing 10% FBS and 1% streptomycin and penicillin at 37°C in 5% carbon dioxide, as described previously [28,29]. Toxicity studies were performed on the optimized formulations, and the results were compared with those obtained among the control cells. The cells were treated with various concentrations (0.1–10 µM) of AgNPs–CTT [30], AgNPs–OCT, and AgNPs–OCT–Alg for 24 h. The concentrations of all formulas were calculated depending on the molecular weight of silver. Cytotoxicity was examined using a kit (Promega, Madison, WI, USA), as previously described [31].

2.6.2 TNF-α ELISA

After pretreatment with different doses of AgNPs–CTT, AgNPs–OCT, and AgNPs–OCT–Alg (0.1–10 µM) for 2 h, MCF-7 cells were examined. The TNF-α content in the culture medium was quantified using a TNF-α-specific ELISA kit according to the manufacturer's instructions (R&D Systems Inc., Minneapolis, MN, USA) [30].

2.6.3 Cell uptake and displacement studies

The uptake and transport of AgNPs–CTT, AgNPs–OCT, and AgNPs–OCT–Alg in MCF-7 cells were investigated to determine the internalization of SSTR-based AgNPs–OCT into the cells. Furthermore, the AgNPs coupled with OCT and alginate ensured targeting of the nanoformulation, while the alginate wrapping ensured its feasibility for nebulization. A competitive replacement experiment was performed by incubating the AgNPs–OCT for 1 h at 37°C [32]. In brief, MCF-7 cells (1×10^7/mL) were placed in 35 mm culture dishes containing Dulbecco's modified Eagle's medium and incubated at 37°C overnight. The cells were incubated with 10 µM each of AgNPs–CTT, AgNPs–OCT, and AgNPs–OCT–Alg. MCF-7 cells were used as a model for SSTR expression [33]. Moreover, the groups that received AgNPs–OCT and AgNPs–OCT–Alg were also incubated with 100 µM free OCT 30 min prior to incubation with the nanoparticles, which led to receptor saturation with OCT *via* competitive replacement. This step aimed to confirm that AgNPs–OCT and AgNPs–OCT–Alg could be displaced from SSTRs by free OCT. The cells were then washed twice with Dulbecco's phosphate-buffered saline, centrifuged at 300 g (180.5°C) for 10 min, and placed in 5 mL glass vials. ICP-OES

was used to assess the concentration of silver ions (Ag^+) [34,35]. Briefly, each AgNP sample (0.5 mL) was mixed with 0.2 mL of freshly prepared aqua regia and diluted to 5 mL with Millipore water. ICP-OES was performed using a JY-70 PLUS (Jobin Yvon Instruments SA Inc.) to determine the quantity of Ag^+ in the digested cells. Ag^+ concentrations of 1, 10, and 100 ppm were used as standards. The concentration of AgNPs in solution was calculated by dividing the number of silver atoms per particle by the estimated concentration of Ag^+ [14,36]. The ICP-OES principle is used to determine the quantity of metals in a sample by measuring the amount of light emitted at different wavelengths [37]. The amount of Ag^+ was calculated using a Microsoft Excel sheet, as reported previously [35].

2.7 Experimental animals

The animal experiments were conducted at the Pharmacology Research Laboratory, College of Pharmacy, Qassim University (Buraydah, Saudi Arabia). The study protocol was approved by the Institutional Animal Ethics Committee Deanship of Scientific Research, Qassim University, Saudi Arabia (approval number: 2019-2-2-I-5551). A histamine chamber (Plexiglas) was prepared (with the following dimensions: length 32 cm, width 15 cm, and height 28 cm) to expose four rats to the prepared AgNP formulations. The nebulizer inlet carried AgNPs to the rats, and the outlet tube maintained the optimum pressure inside the chamber for inhalation. Millipore water was used to prepare all nebulizing solutions. This experiment was carried out on 12 Sprague–Dawley rats of both sexes obtained from the College of Pharmacy Animal House. The rats were 7 weeks old, with body weights of 200–250 g, and were provided a rodent chow diet and water *ad libitum*. All rats were acclimatized to the laboratory environment in clean cages for 5 days and maintained daily with a 10–14 h photoperiod. The rats were nebulized using a System LS 290 aerosol nebulizer (System Assistance Medical SAS, Villeneuve-sur-Lot, France). This system used room air with appropriate pressures and temperatures to vaporize solutions into a micro-fine aerosol mist that flowed into the tubes of the Plexiglas chamber for the animals to inhale. The rats were distributed equally into groups (the control, AgNPs–CTT, and AgNPs–OCT–Alg groups). Rats in the control group were nebulized with Millipore water, those in the AgNPs–CTT group with AgNPs–CTT, and those in the AgNPs–OCT–Alg group with AgNPs–OCT–Alg. The concentrations of the nanoformulations were 10 µM each. The total dose of each formulation was 1.27 mg/kg [38], and 50 mL of each formulation was used for nebulization

at a rate of 5 mL/h. In each experiment, the nebulizer dosing cup was filled with 10 mL of liquid and nebulized until it dried out; the nebulization was continued for 3 days (within 10 h/day). On the same day, lung tissues were excised and processed [39,40].

2.7.1 Analysis of the biodistribution of the AgNPs–OCT–Alg

The quantity of Ag^+ was analyzed using ICP-OES to determine the amount of inhaled AgNPs–OCT. Lung tissues were homogenized in 86% nitric acid and hydrochloric acid. The homogenized tissue was diluted with phosphate-buffered saline (pH 7.4). The AgNPs–OCT concentration was determined by quantifying the amount of Ag^+ using the ICP-OES technique according to a protocol described in previous studies [41,42].

2.7.2 Ultrastructural examination by transmission electron microscopy (TEM)

Lung specimens were excised and processed (fixed in 2.5% glutaraldehyde for 2 h, post-fixed in 1% osmium tetroxide for 1 h, dehydrated in ethanol, cleared in propylene oxide, and embedded in epoxy resin). After thermal polymerization, ultrathin sections were cut with an ultramicrotome and stained with uranyl acetate and lead citrate [43]. The grids of the ultrathin sections were examined and photographed using a transmission electron microscope (JEOL 1010; JEOL Ltd, Tokyo, Japan) at the Electron Microscopy Unit of the College of Applied Medical Sciences (Qassim University) to identify the ultrastructural details of the alveolar cells [44]. The nanoparticles were electron-dense with characteristic round shapes and equal in size.

2.7.3 Statistical analysis

The data are presented as the mean of at least three experiments with their standard deviations. Comparisons of single or multiple samples were performed using *t*-tests. The analyses were performed using SPSS Statistics version 27 (IBM Corporation, Armonk, NY, USA). Analysis items with $p < 0.05$ were considered statistically significant.

3 Results

The AgNPs–CTT formulation was prepared and conjugated to OCT to enable it to specifically target $SSTR_2$.

The prepared AgNPs–CTT–OCT or AgNPs–OCT was coated with alginate (*via* a 1% aqueous sodium alginate solution) to yield AgNPs–OCT–Alg for easy delivery to the lungs by inhalation in rat models in a histamine chamber (Figure 1a–c) (Plexiglas). The nebulizer inlet transported the AgNPs–OCT–Alg formulation to the rats (Figure 1b and c). The prepared AgNPs–CTTs were uniformly shaped and brown in color. The brown color turned darker after conjugating the AgNPs–CTT with OCT. The AgNPs–CTT was coupled with OCT at its N-terminus, forming an amide bond between the OCT and the citrate carboxyl group of the AgNPs–CTT. The reaction can be progressed at a slightly acidic or neutral pH to avoid reaction with the lysine side-chain amino group (NH_2) of OCT, which (lysine-NH_2) is essential for activity (Figure 1d) [17,45].

Table 1 shows the initial Ag^+ and Ag^0 concentrations in AgNPs following NP formation, as measured by ICP-OES. The yield% was calculated for Ag^0 synthesized in the AgNPs–CTT, AgNPs–OCT, AgNPs–OCT–Alg to be 2.82 ± 0.016 mg/100 mL ($\approx 77.9\%$), 2.43 ± 0.21 mg/100 mL ($\approx 67.12\%$), and 2.166 ± 0.19 mg/100 mL ($\approx 59.83\%$), respectively.

3.1 Size, ζ potential, and surface morphology

A dynamic light scattering zetasizer nano was used to record the sizes of the AgNPs–CTT, AgNPs–OCT, and AgNPs–OCT–Alg, which were determined to be 22.77 ± 1.1, 78.77 ± 2.3, and 155.99 ± 5.2 nm, respectively. The ζ potentials of the three formulations had surface charge values of -40.17 ± 2.0, -14.13 ± 1.3, and $+16.17 \pm 1.3$ mV, respectively (Figure 2).

3.2 Ultraviolet-visible spectroscopy

Ultraviolet-visible spectroscopy (UV-VIS) was used to record the wavelengths of maximum absorption (λ_{max}) of the AgNPs–CTT, AgNPs–OCT, and AgNPs–OCT–Alg, which were determined as 430.7 ± 2.99, 447.8 ± 2.93, and 450.8 ± 3.5 nm, respectively. The UV-VIS spectrum of the AgNPs–CTT showed redshifts of 17 and 3 nm in the SPR peaks for both AgNPs–OCT and AgNPs–OCT–Alg, respectively (Figure 3) [35].

3.3 *In vitro* treatment of MCF-7 cells with AgNP formulations

The cytotoxic effects of the AgNPs–CTT, AgNPs–OCT, and AgNPs–OCT–Alg on MCF-7 cells were evaluated using
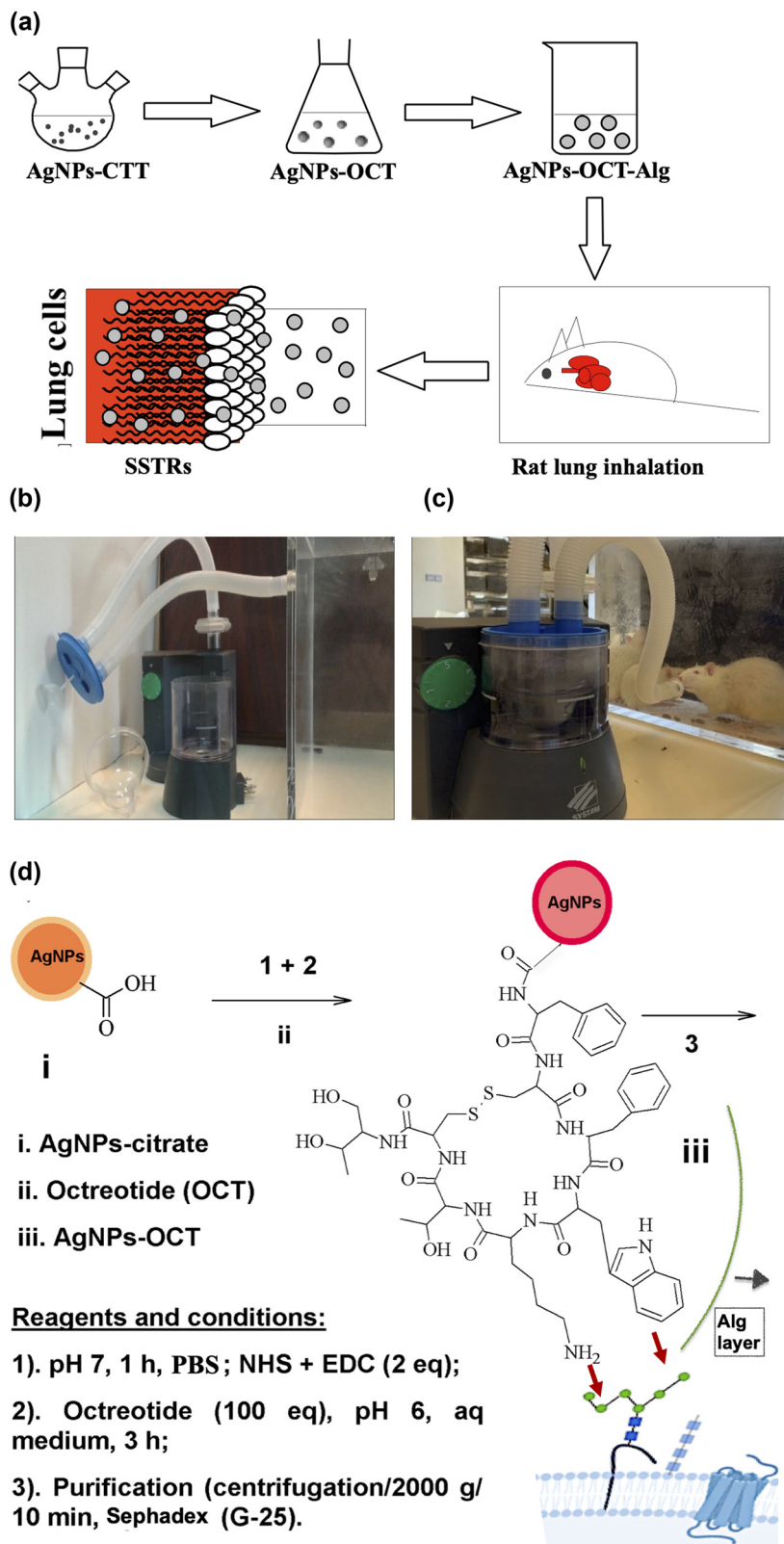
Figure 1: (a) Schematic diagram of AgNPs−OCT−Alg preparation and delivery to lung cells. (b and c) Nebulization of AgNPs−OCT−Alg among rats. (d) Schematic diagram of AgNPs−OCT synthesis; the AgNPs−OCT formed were coated with alginate for delivery to the lung cells and the proposed manner in which OCT fits into the SSTRs by interactions between lysine and phenylalanine.

Table 1: The yield percentage of Ag° in AgNPs after conversion of Ag$^+$ to Ag^0

Sample	Concentration (mg/100 mL)	Yield % (conversion%)
Ag$^+$ (initial concentration)	3.62 ± 0.1	—
AgNPs–CTT	2.82 ± 0.016	77.9
AgNPs–OCT	2.43 ± 0.21	67.12
AgNPs–OCT–Alg	2.166 ± 0.19	59.83

different concentrations (0.1–10 µM) of the nanoparticle formulations. The extent of cancer cell proliferation significantly decreased after treatment with different AgNP formulations compared to the proliferation of control cells (Figure 4). In the model cytotoxicity evaluation experiment involving the MCF-7 cell lines, the results showed that treatment of the breast cancer cell lines with AgNPs–CTT, AgNPs–OCT, and AgNPs–OCT–Alg significantly reduced cell proliferation in a concentration-dependent manner (Figure 4). The degree of proliferation
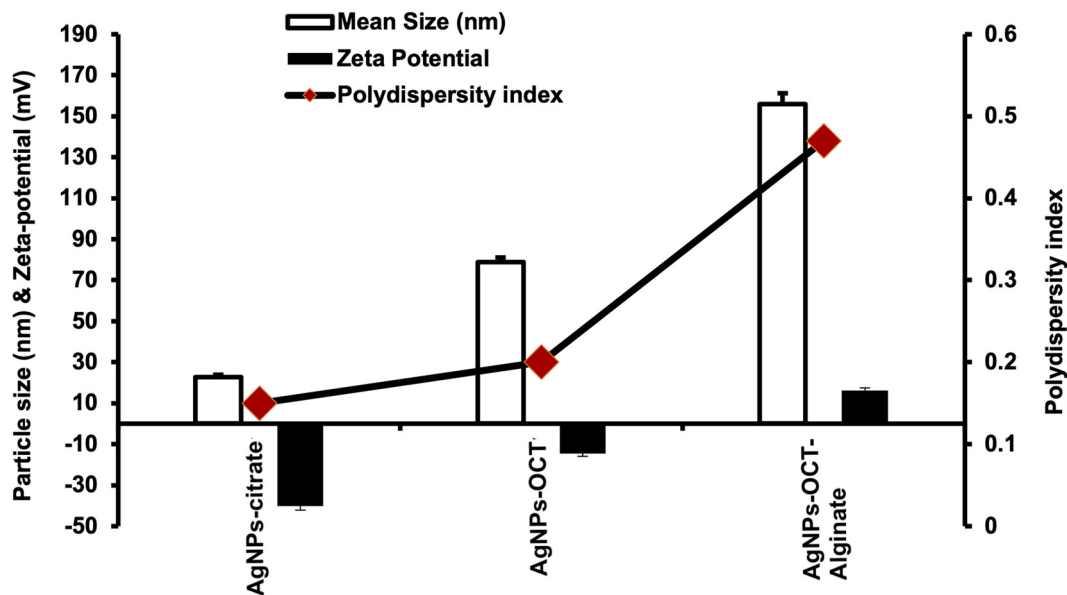
Figure 2: Size distributions (nm), ζ potentials (mV), and polydispersity indices of the AgNPs–CTT, AgNPs–OCT, and AgNPs–OCT–Alg.
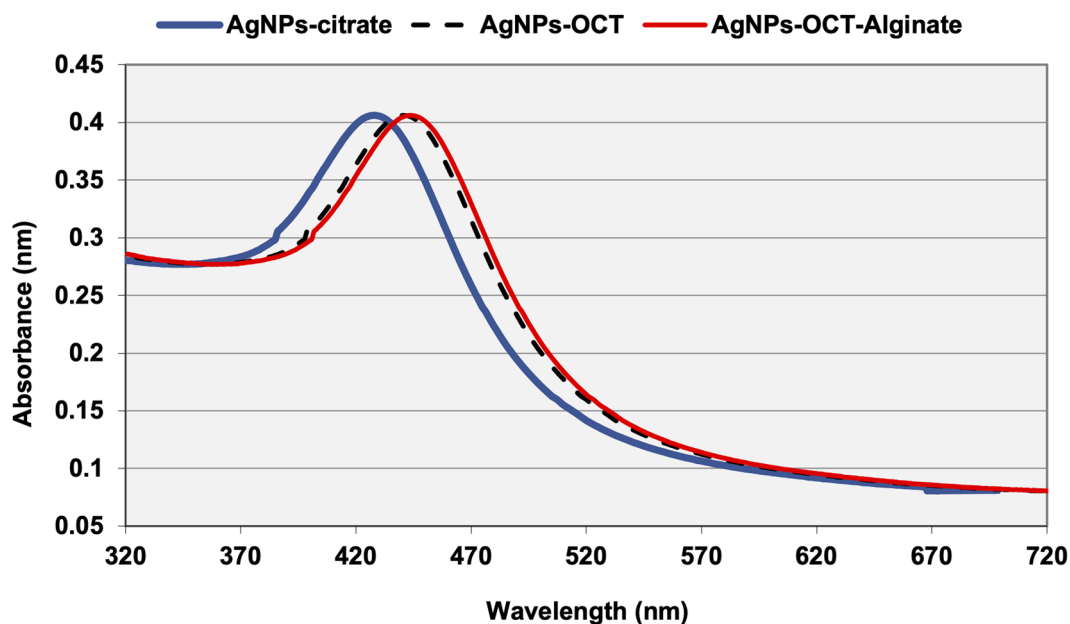
Figure 3: UV-Vis spectra of AgNPs–CTT, AgNPs–OCT and AgNPs–OCT–Alg. The AgNPs–OCT and AgNPs–OCT–Alg showed redshifts in their SPR peaks.
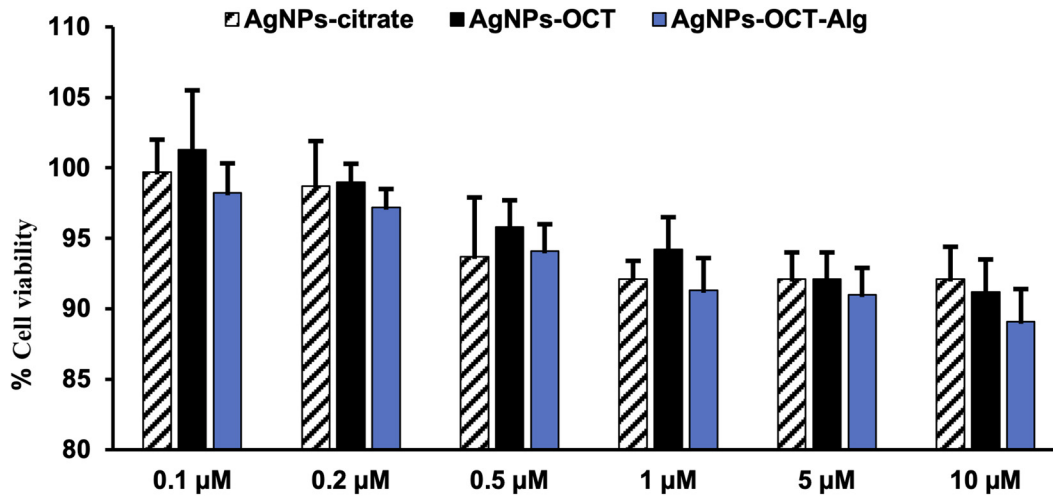
Figure 4: Effects of different AgNP formulations on MCF-7 cell proliferation after treatment with different concentrations (0.1–5 µM) of AgNP formulations. The results are representative (mean ± standard error of the mean) of triplicate experiments; data without an asterisk differ, *$p < 0.05$ *versus* untreated cells (control cells). All formulations showed no toxicity, while concentrations of 1–5 µM showed significant inhibition of cell proliferation ($p < 0.05$).

was significantly reduced when MCF-7 cells were treated with each of the AgNP formulations for 24 h. The AgNPs–OCT–Alg formulation was more efficient in reducing cell proliferation than the AgNPs–OCT, and AgNPs–CTT formulations after 24 h of incubation (Figure 4). Treatment of the MCF-7 cell lines with 5–10 µM of each of the AgNP formulations revealed that treatment with AgNPs–OCT and AgNPs–OCT–Alg inhibited the proliferation of all cells compared to the cells treated with only the AgNPs–CTT [46].

In addition, the protein levels of TNF-α were determined *via* ELISA. Treatment with 0.1–10 µM of AgNP preparations significantly decreased the production of TNF-α in the MCF-7 cell lines compared with control cells (Figure 5). The cell cultures treated with 5–10 µM each of the AgNP formulations showed significant suppression ($p < 0.05$). The level of TNF-α production was higher in the 0.1 µM group than in the control group. The levels of TNF-α decreased significantly in the cells treated with 5 and 10 µM each of
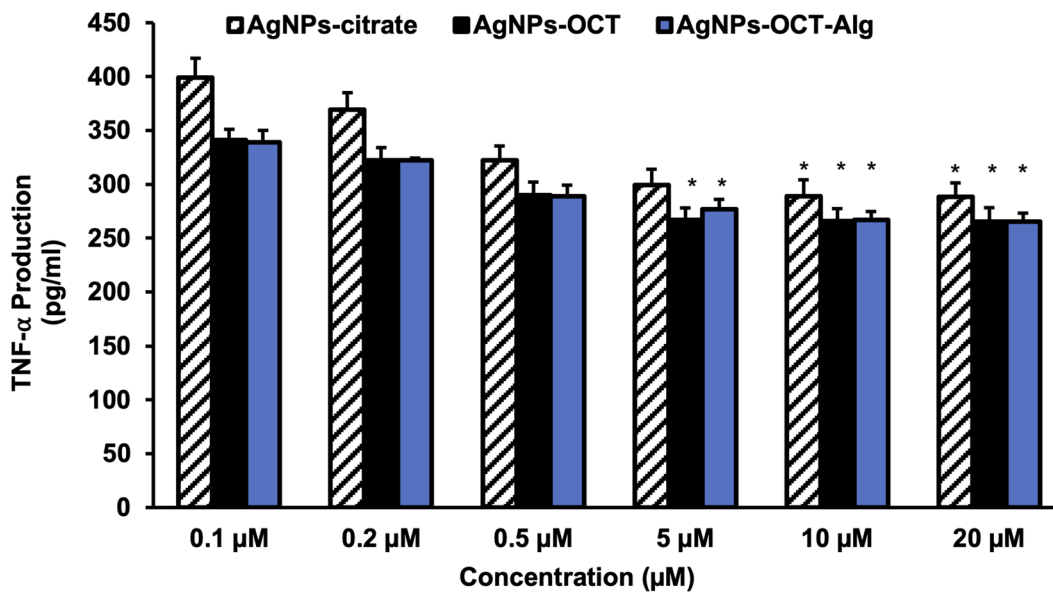

Figure 5: Production of TNF-α after treatment with AgNP formulations in MCF-7 cells. The results are representative (mean ± standard error of the mean) of triplicate experiments. Data without an asterisk differ and concentrations of 5–10 µM showed significant TNF-α inhibition ($p < 0.05$). *$p < 0.05$ *versus* untreated cells (control cells).

the AgNPs–CTT, AgNPs–OCT, and AgNPs–OCT–Alg ($p < 0.05$) formulations compared with the cells in the control group. These results confirmed that the nanoparticles could be used as cancer formulations at concentrations >5 μM.

Moreover, ICP-OES showed higher levels of internalization of AgNPs–OCT also into the MCF-7 cells. The cellular uptakes of 10 μM formulations of AgNPs–CTT, AgNPs–OCT, and AgNPs–OCT–Alg were determined *via* ICP-OES after 60 min of incubation. The control MCF-7 cell lines showed negligible quantities of internalized AgNPs, and AgNPs–CTT showed nonsignificant levels of random internalization ($p > 0.05$). AgNPs–OCT showed more significant levels of internalization at $387 \pm 23.6 \times 10^3$ per cell ($p < 0.001$). The amount of accumulated AgNPs decreased to $243 \pm 12.6 \times 10^3$ in the cells treated with AgNPs–OCT–Alg ($p < 0.05$). Furthermore, the amounts of internalized AgNPs decreased to $156.88 \pm 21.4 \times 10^3$ and $126 \pm 11.7 \times 10^3$ in the AgNPs–OCT and AgNPs–OCT–Alg treated groups, respectively ($p < 0.001$), when the receptors were occupied by 100 μM of free OCT (Figure 6).

3.4 *In vivo* inhalation of AgNP formulations

The images of inhaled AgNPs in different groups are presented as photomicrographs from lung sections stained with toluidine blue (Figure 7a–c). Figure 7b shows an image of inhaled AgNPs–CTT (arrow) and Figure 7c shows an image of inhaled AgNPs–OCT–Alg (arrow). Also, Figure 7d–f presents the TEM photomicrographs of the ultrathin lung sections. Figure 7e presents an image of inhaled AgNPs–CTT (arrow) and Figure 7f shows an image of inhaled AgNPs–OCT–Alg (arrow). Figure 7g shows the proportions of inhaled AgNPs–CTT, AgNPs–OCT, and AgNPs–OCT–Alg as determined *via* ICP-OES. Figure 7a shows the absence of inhaled AgNPs in the lungs; Figure 7b shows an image with a low amount of inhaled AgNPs–CTT (red arrow), while Figure 7c shows an image with a significant amount of inhaled AgNPs–OCT–Alg (red arrow) ($p < 0.05$). The results were confirmed by TEM photomicrographs of ultrathin lung sections (Figure 7d–f). Figure 7d shows the absence of inhaled AgNPs, Figure 7e displays a low amount of inhaled AgNPs–CTT (red arrow), while Figure 7f shows a higher amount of inhaled AgNPs–OCT–Alg (red arrow), which confirms our hypothesis. In addition, the nanoparticles shown in Figure 7e and f were smaller than the artifacts appearing as irregular black spots (blue arrows) in Figure 7d. These results were also confirmed by ICP-OES, which determined the amount of inhaled AgNPs in lung cells. Figure 7g demonstrates the proportion of inhaled AgNPs–CTT, AgNPs–OCT, and AgNPs–OCT–Alg as determined by ICP-OES. The proportion of inhaled AgNPs–OCT–Alg was 0.416 ± 5.7 mg/kg$_{tissue}$, which confirmed active targeting of the lung tissue, while the proportion
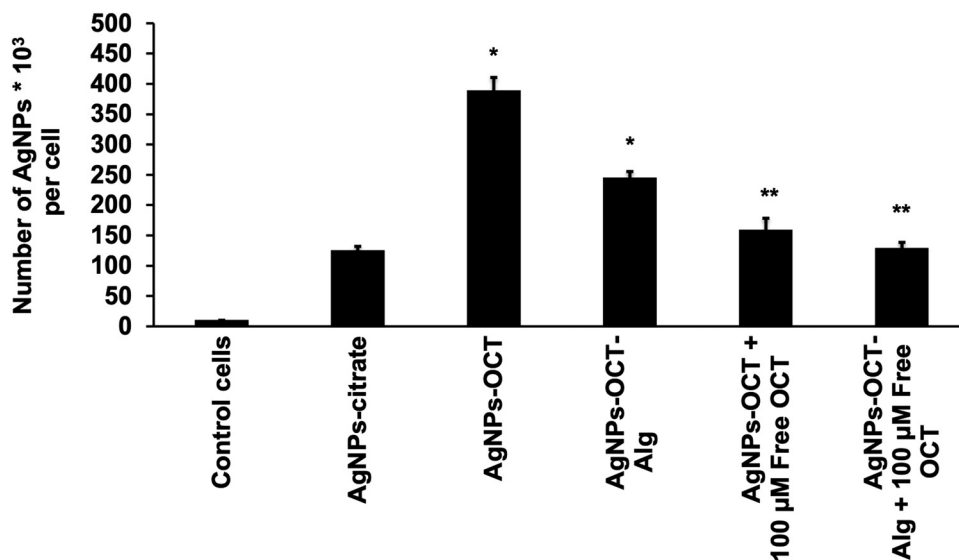

Figure 6: Cellular uptake of the AgNPs–CTT, AgNPs–OCT, and AgNPs–OCT–Alg was determined by ICP-OES and cell counting after 60 min of incubation. The administered concentrations of AgNP formulations were 10 μM. *Statistically significant ($p \leq 0.05$; analysis of variance/ Tukey's test). The AgNPs–OCT and AgNPs–OCT–Alg specifically targeted SSTR$_2$, while the level of internalization was decreased because SSTR$_2$ was occupied by free OCT. *$p < 0.05$ *versus* untreated cells (control cells), **$p < 0.001$ *versus* the group of AgNPs–OCT and AgNPs–OCT–Alg.
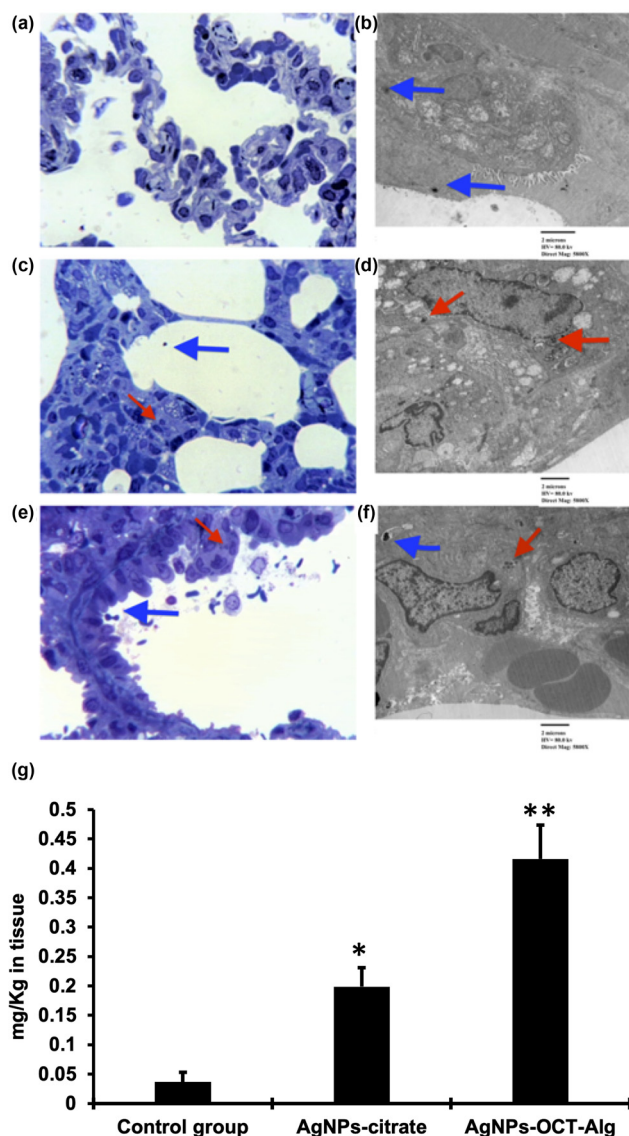
Figure 7: (a–c) Photomicrographs of lung sections stained with toluidine blue. Panel b shows inhaled AgNPs–CTT (red arrow) and panel c shows inhaled AgNPs–OCT–Alg (red arrow); (d–f) transmission electron microscopy (TEM) photomicrographs of ultrathin lung sections; the irregularly shaped, comparatively larger black spots are artifacts shown by blue arrows; (e) inhaled AgNPs–CTT (red arrow); (f) inhaled AgNPs–OCT–Alg (red arrow); (g) the proportions of inhaled AgNPs–CTT, AgNPs–OCT, and AgNPs–OCT–Alg as determined by ICP-OES. The concentrations of AgNPs were 10 µM. *$p < 0.05$ *versus* control group, **$p < 0.001$ *versus* AgNPs–CTT group and control group.

of inhaled AgNPs–CTT was $0.199 \pm 3.21\,\text{mg/kg}_{\text{tissue}}$, which indicated nonspecific uptake leading to Ag^+ accumulation. ICP-OES showed that AgNPs–OCT–Alg inhalation led to a higher amount of Ag^+ accumulation compared with AgNPs–CTT inhalation ($p < 0.001$; analysis of variance/ Tukey's *post-hoc* test). The AgNPs–CTT, AgNPs–OCT, and

AgNPs–OCT–Alg formulations were all inhaled after nebulization, and the lung tissues were histologically examined for the presence of AgNPs. Nonspecific and random accumulation of AgNPs–CTT in the lung occurred due to rapid uptake by alveolar cells [47].

4 Discussion

In the present study, we modified a previously described chemical reduction technique to synthesize citrate-reduced and capped nanoparticles (AgNPs–CTT) [48]. Due to the reduction of Ag^+, neutral silver atoms were formed by the nucleation of Ag^+ [49] according to the redox equation, based on the reduction potential of the bulk starting material, as shown below:

$$Ag^+ + e^- \rightarrow Ag^0(1)(ac)(s)$$
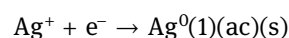
Seeding and nucleus production were more likely to occur when Ag^+ was used at low concentrations (submillimolar range), as used in this study. Constant stirring of the reaction solution was necessary to prevent collision and the formation of silver nuclei in the solution. Temperature and pH are also important factors in the preparation; however, they also affect synthesis and product yields, resulting in changes in the nanoparticle size, charge, and polydispersity [36]. The reduced AgNPs–CTT provided strongly reactive, thermodynamically stable, fully reduced, appropriately citrate-capped AgNPs with high antioxidant potential, functional, specific, and ready-to-conjugate nanopreparations. The reduction process yielded characteristically superior quality by designing nanoparticles for further use in the preparation. Bulk materials are very sluggish in reacting and producing conjugates, have been improved to highly chemically reactive, energy-absorbing nanopreparations, and have provided the functional material for further use in preparing desired nanoparticles with site-specific targeting. The yield% was calculated for Ag^0 synthesized in the AgNPs–CTT, AgNPs–OCT, AgNPs–OCT–Alg using ICP-OES to be $2.82 \pm 0.016\,\text{mg}/100\,\text{mL}$ ($\approx 77.9\%$), $2.43 \pm 0.21\,\text{mg}/100\,\text{mL}$ ($\approx 67.12\%$), and $2.166 \pm 0.19\,\text{mg}/100\,\text{mL}$ ($\approx 59.83\%$), respectively. Although the yield percentage does not reach 100% with the current synthesis method, while an acceptable yield percentage was attained for all kinds of AgNPs. Inconsistencies between reported and theoretical Ag inputs can also be ascribed to Ag^+ or AgNPs adsorption on centrifuge tubes or pipettes, volume loss, and transportation during sample transfer for dilution and quantification [25].
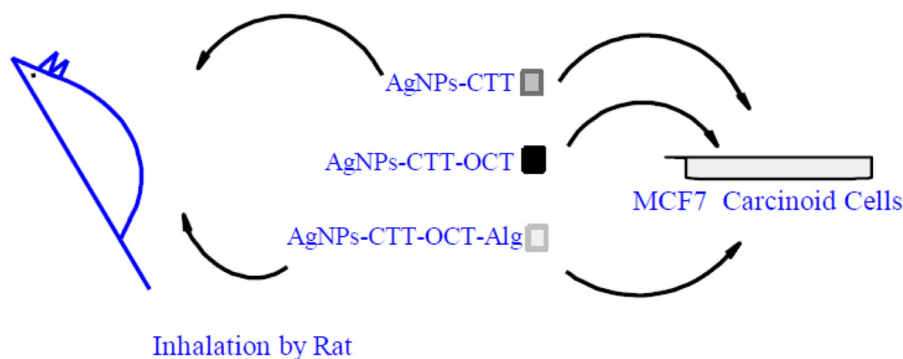
Figure 8: Schematic representation of the different types of AgNPs applied in *in vitro* and *in vivo* experiments.

Nanoparticle delivery to the lungs suffers from two significant drawbacks, one of which occurs prior to administration and the other after administration. First, nanoparticle aggregation occurs more frequently in an aqueous medium after long-term storage. Second, the smaller-sized nanoparticles are quickly exhaled unless they are delivered and deposited deep inside the lungs [50,51]. The AgNPs–OCT–Alg was designed as a formulation carrier to overcome the problems associated with pulmonary delivery and the aggregation of nanoparticles to achieve better delivery and deposition in the lungs. The formulated nanoparticles incorporated an alginate layer, which acted as an outer coat and worked as a better carrier than the nanoparticulate formulations, AgNPs–CTT and AgNPs–OCT, which are easily exhaled upon administration among the animals. The alginate-coated AgNPs–OCT forming AgNPs–OCT–Ag was a facile delivery carrier for nebulization. There was no chemical bonding between the outer alginate coating and the nanoparticles themselves, as the alginate layer was merely a physical wrap around the nano-entity. Due to the weight and size of the AgNPs–OCT–Alg, it was successfully delivered into the lungs without exhalation, which was observed with the non-coated AgNPs–CTT and AgNPs–OCT formulations [52]. Moreover, the alginate wrapping was soluble in aqueous media. The alginate wrappings of AgNPs–OCT–Alg only served as a medium for effective delivery and dispersion. Nonetheless, the fragility of the alginate coating was demonstrated by the UV absorption maxima for AgNPs–OCT and AgNPs–OCT–Alg. Both of these formulations showed near similar values at 447.8 ± 2.93 and 450.8 ± 3.5 nm (Figure 3), respectively, wherein the λ_{max} determined *via* UV-VIS of both the nanoparticle formulations, AgNPs–CTT and AgNPs–OCT, was nearly unaffected by the alginate coating, with a 3 nm shift of the absorption maxima. The alginate wrapped around the nanoparticles easily and quickly dissipated into the aqueous-based media in the lungs of the animal models. The

AgNPs–CTT and the AgNPs–OCT–Alg treatment groups were compared to confirm the feasibility of nonspecific and specific delivery of the carrier-based formulations. The alginate coating was only used to facilitate the inhalation of the AgNPs–OCT formulation, which was not effectively inhaled. The alginate layer (in the AgNPs–OCT–Alg formulation) facilitated delivery through the inhalation route and nearly diminished the exhalation of the AgNPs–OCT formulation. The alginate wrapping was replaced in aqueous media, both in the *in vivo* (inhalation among the rats) and *in vitro* (MCF7 cancer cells) models, and resulted in internalization at higher levels than the non-OCT citrate-capped formulation (AgNPs–CTT) (Figure 8). The SPR redshifts were observed due to the coupling of AgNPs–CTT with the OCT and alginate wrapping of the AgNPs–OCT. The optical properties of all AgNPs depended on the diameters of the preparations, and the peaks shifted toward longer wavelengths (redshift); therefore, the large-sized particles had larger optical cross-sections, and their albedo (the reflected fraction of SPR) increased similar to the redshifts with the increased size [35]. In the case of the AgNPs–OCT–Alg, the redshift was 3 nm, which signified the least changes in the SPR shifts (nearly no structural change, except noncovalent coating between the AgNPs–OCT and the AgNPs–OCT–Alg). The final products were citrate-capped nanoparticles (AgNPs–CTT), OCT-chemically-conjugated-to-citrate-nanoparticles (AgNPs–OCT), and the alginate-wrapped AgNPs–OCT–Ag. The absorption for the covalently linked alginate was much higher. However, in this case, the AgNPs–OCT was treated in an alginate solution, dried to produce the alginate-wrapped nanoparticles (a thin coating/film around the AgNPs–OCT) as AgNPs–OCT–Alg, and the chemically conjugated (absorption being higher) and nonconjugated (with no chemical bond) formulations showed comparatively low levels of absorption. As the nanoparticles were in aqueous media, alginate displacement yielded very little change in the

absorption, as in this spectrum recording event, alginate was displaced with enough water in the medium. All other UV recordings were also performed using water as the medium. All three preparations were also of different colors. The smaller difference of 3 nm was a result of the effect of alginate. UV spectra were recorded for the AgNPs–OCT–Alg product, a characterized material with size, charge, and shape specifications. The small shift (redshift) of <3 nm was in agreement with the layer-by-layer coating of AgNPs reported by Detsri et al. [53].

Therefore, due to nanoparticles, AgNPs–OCT–Alg increased in size and was found to be more effectively delivered into the lungs through inhalation. As reported previously, for a carrier of suitable (nano-metric) size, entrapment in the lungs is better for achieving pulmonary deposition (Figure 9) [54]. The size of the AgNPs–OCT–Alg was intended to be increased, and the size of AgNPs increased from 22.77 ± 1.1 nm for the AgNPs–CTT to 78.77 ± 2.3 nm for the AgNPs–OCT. Finally, the coated nanoformulation, AgNPs–OCT–Alg, resulted in an average size of 155.99 ± 5.2 nm, which could be effectively delivered to the lungs. The alginate coating has been proposed to be dissolved after formulation delivery since there is no chemical bonding between the alginate and the surface-located OCT of the AgNPs–OCT, except for the physical wrappings of the alginate coating around the AgNPs–OCT. However, a chemical bond forms between the AgNPs–CTT and OCT to produce AgNPs–OCT from the AgNPs–CTT based carboxylate and the NH_2 group of the OCT forming an amide linkage, which is stable enough for delivery and deposition [45,55]. The Ag^+ internalizations of the formulations, AgNPs–CTT and AgNPs–OCT–Alg, were compared in terms of site-specific delivery and Ag^+ internalizations by the alginate-coated nanoparticles and noncoated, non-OCT-capped AgNPs–CTT. There was no need to compare the AgNPs–CTT and AgNPs–OCT, as the OCT coating itself was target-specific (targeting SSTRs) and was expected to yield higher levels of internalization of Ag^+.
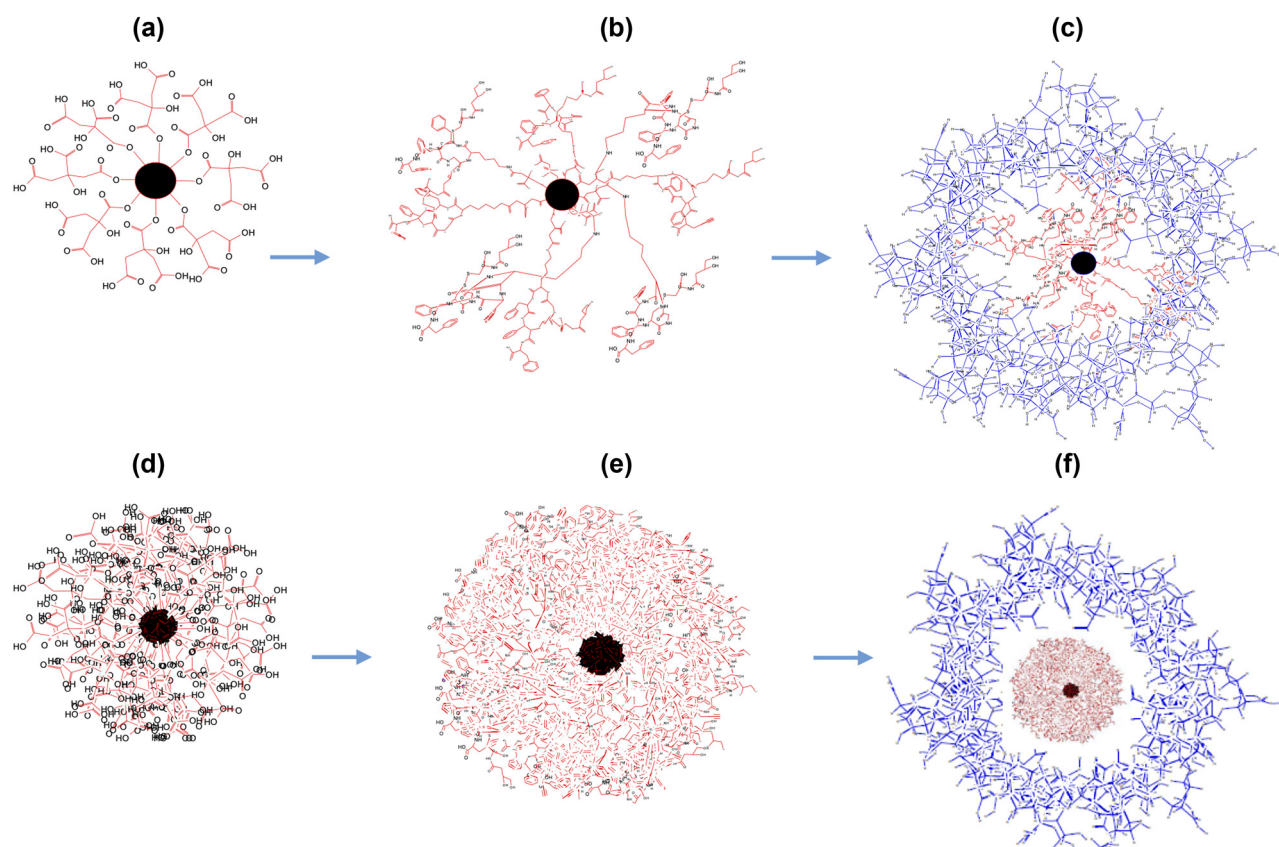

Figure 9: Structural representations of the AgNP nanocarriers; (a–c) 2D renderings, (a) AgNPs–CTT (citrate bound to the nanoparticle, nanoparticle depicted in black). (b) AgNPs–OCT (OCT covalently bound to citrate, CTT). (c) AgNPs–OCT–Alg (no chemical bonding; instead, physical wrapping of the alginate around the AgNPs–OCT. Alg: alginate, coatings shown in blue). 3D renderings of the AgNPs. (d–f) 3D renderings, (d) AgNPs–CTT. (e) AgNPs–CTT–OCT. (f) AgNPs–OCT–Alg. Alginate coatings are not chemically bound. The core of the formulated AgNPs–OCT is shown in red, while the surrounding alginate wrapping is shown in blue.

The AgNPs–OCT–Alg could be considered as an innovative therapy for lung diseases, as it imparts SSTR analogs and several drugs with the potential for delivery due to the capacity for attachment to the AgNPs–CTT nanopreparation. All types of AgNP formulations (AgNPs–CTT, AgNPs–OCT, and AgNPs–OCT–Alg) were successfully prepared, characterized, and biologically tested in the present study. The conjugation of the AgNPs–CTT with OCT and alginate coatings were analyzed and confirmed through spectrophotometric analyses, morphological observations, and ζ potential measurements. The AgNPs–OCT formulation was optimized for lung delivery through dispersion in a sodium alginate aqueous solution (1%) as a coat around the AgNPs–OCT. The successful coupling of AgNPs–CTT with OCT and alginate coating to form AgNPs–OCT–Alg showed a surface charge of −40.17 ± 2 mV, with an increase to −14.13 ± 1.3 mV for AgNPs–CTT, and AgNPs–CTT–OCT (AgNPs–OCT), to a positive (inverted sign) potential of +16.17 ± 1.3 mV upon alginate treatment. The changes in value and reversal in the ζ potential sign confirmed the successful coupling of OCT and coating of alginate onto the surface of the AgNPs–CTT and the AgNPs–OCT wrappings, respectively. The AgNPs–OCT preparation showed higher stability due to its high ζ potential [56]. These results were in agreement with the results obtained by Lu *et al.*, who established that distinct stability is achievable when the ζ potential values are approximately within +10 to −10 mV [57]. Initial preparation involving aqueous media reaction between TSC and AgNO$_3$ produced AgNPs–CTT, which were brown and produced the characteristic SPR absorption bands [58].

Figure 9 presents plausible 2D and 3D shapes, physical, and chemical bonding representations of the AgNPs–CTT, AgNPs–OCT, and AgNPs–OCT–Alg nanopreparations throughout their stages of preparation and developmental processes (Figure 9a–f). The present study aimed to actively target the alginate-coated AgNPs (AgNPs–CTT–OCT–Alg or AgNPs–OCT–Alg) to SSTRs using the surface-attached ligand of SSTR (OCT) as the site-directed specific ligand for active and accurate delivery to the lung tissue.

To study the cellular uptake and displacement of all formulated AgNPs, we used MCF-7 cells as a model cell line that express SSTRs, which specifically express SSTRs as studied previously at our laboratory [59]. The expression of SSTR$_2$ in MCF-7 cells was confirmed by binding with OCT-conjugated fluorescein isothiocyanate, using BON-1 cells as positive controls [44]. Besides, the mRNA level of SSTR$_2$, as determined by reverse transcription polymerase chain reaction assay, was significantly higher in MCF-7 cells than in BON-1 cells as positive controls. The results confirmed that the AgNPs–OCT–Alg was effective

in delivering the formulation to cell lines under *in vitro* conditions, and successfully and effectively delivered the AgNPs–OCT–Alg formulation to effectively deposit into the lung tissues within the optimal concentration limits, between 5 and 10 μM, for *in vivo* anticancer activity in rat models. The lowest concentration that induced anticancer activity *in vivo* has also been investigated [46,60]. The half-maximal inhibitory concentration (IC$_{50}$) values were observed at 5–10 and 10 μM under *in vitro* and *in vivo* conditions, respectively. Moreover, the IC$_{50}$ for AgNPs–CTT was also found to be less than 20 μM [30]. As TNF-α promotes the proliferation of cancer cells [61], it was also observed that AgNPs–OCT significantly inhibited TNF-α production. Moreover, the cells were affected by the minimum concentration of AgNPs–OCT. A higher concentration of all AgNP preparations (10 μM) was used to assess their antiproliferative activity, as suggested by Xu *et al.* [62]. The researchers confirmed that the toxicity of AgNPs–CTT increased at concentrations >10 μg/mL, while AgNPs–CTT (5 μg/mL) tended to show comparatively reduced levels of cytotoxicity. Moreover, ICP-OES showed higher levels of internalization of AgNPs in the form of AgNPs–OCT in *in vitro* tests due to the direct interaction between OCT and SSTR$_2$ expressed on the surfaces of the MCF-7 cells. In addition, the weak interactions between AgNPs–OCT–Alg and MCF-7 cells due to alginate coating on the surface of the nanoparticles initially formed a barrier between the OCT binding sites and SSTR$_2$.

The selectivity for SSTR$_2$ was confirmed based on the occupation of the receptors with 100 μM free OCT, and the binding of the nanoparticulate formulations to the receptor was observed to be significantly reduced under these conditions [59,63,64]. Moreover, these results showed lower levels of internalization of the nanoparticle formulations in the cells, as binding was reduced in the presence of free OCT, which preferentially and quickly blocked and occupied the SSTR$_2$. The AgNP formulations were applied at concentrations described in a previous report published by Xu *et al.* [62]. The levels of TNF-α also showed a marked decline, as determined *via* ELISA. The AgNP formulations at concentrations of 0.1–10 μM significantly decreased TNF-α production in MCF-7 cells. Moreover, the 10 μM AgNP formulations showed the most significant levels of suppression of TNF-α, with no additional decrease in TNF-α production at higher nanoparticle concentrations [30]. This significant decline in TNF-α production indicated that AgNPs–OCT could be an effective material to target cancer cells, particularly, breast cancer cells, while decreasing TNF-α production. The results obtained also showed promise in targeting breast cancer since the AgNPs–OCT and AgNPs–OCT–Alg were better designed for active targeting with an increased cellular accumulation of nanoparticles. Active targeting of

breast cancer is a promising strategy for efficient drug delivery [65]. Many target sites can be reached in breast tissue for site-specific and active targeting [65]. $SSTR_2$ and $SSTR_5$ are expressed in neuroendocrine breast cancer and are considered potential targets for the treatment of breast cancer in the future [66,67]. Li *et al.* [68] reported a novel active targeting approach established on L-type amino acid transporter 1 (LAT1) expressed in a range of cancers. Poly (lactic-*co*-glycolic acid) nanoparticles have also been investigated among MCF-7 cells. Compared to unmodified nanoparticles, LAT1-targeting nanoparticles showed a considerable increase in cellular uptake and cytotoxicity.

The AgNPs–OCT–Alg formulation is stabilized primarily by the adsorption of alginate (Alg) onto the surface of AgNPs–OCT [69]. The produced nanomaterials (AgNPs–CTT and AgNPs–OCT) are comparatively smaller in size and lighter in weight, which implies that upon inhalation, these AgNPs preparations will be either partially or completely exhaled without deposition into the lungs. The alginate coating provides additional increases in layering, weightage, thickness, and size to yield a larger and effective nanoscale carrier (approximately, 155.99 nm) with good flow properties to target the required regions in the lungs and with minimum or no exhalation of the formulation. After accumulating in the lungs, the AgNPs–OCT–Alg attaches to the surface of the pulmonary alveoli, and the coated nanoparticle formulation is presented in the vicinity of the epithelial cells for delivery into the lung cells [70]. These sizes of deposition are in agreement with the report published by Brown [71], which stated that particle deposition in the respiratory tract occurs mainly by diffusion, sedimentation, and impaction. The total amount deposited in the respiratory tract follows a "*U*-shaped" curve, with a minimum deposition of nanoparticles with sizes ranging between 0.1 and 1.0 μm, with enhanced diffusive deposition. Han *et al.* [72], formulated gold nanoparticles (AuNPs) and studied the effect of size on the biodistribution of AuNPs among Sprague–Dawley rats *via* inhalation. The researchers used small AuNPs (with diameters of 13–105 nm and concentrations of 12.8–13.7 μg/m). The animals were exposed to AuNPs for 5 days (6 h/day). They found that the exposed rats exhibited no toxic responses to AuNPs. Regardless of size, both small and large AuNPs were deposited in the lungs of rats. The biodistribution of small AuNPs from the lungs to secondary target organs was significantly higher when compared to those of large AuNPs. Moreover, nanoparticles with diameters smaller than 100 nm were also probably deposited [73,74].

Upon reaching the lung tissues, the alginate layer (Alg) is expected to dissolve slowly in the presence of aqueous media based on the presence of water/moisture,

swelling, and removal of the alginate coating, and AgNPs–OCT is released from the wrapped coating of alginate. The AgNPs–OCT escapes the initial mucociliary clearance of the lungs and crosses the epithelial layer to target lung cancer through OCT, and cancer cell surfaces present SSTR interactions for deposition deep in the lung tissues. Alginate, a highly hydrophilic ionic material (in the form of Alg), is expected to dissolve within a short time, as recorded in the UV-VIS absorption experiments as well as in the tests of the accumulation of AgNPs in nanoformulation, wherein the coated material accumulated to a lesser extent than did the free OCT.

Healthy rats were used for the *in vivo* study as reported to express the $SSTR_2$ [75], which was our target to prove. The OCT ligand-coated AgNPs–OCT was capable of specifically targeting SSTRs located in the lung tissues. The ability of these AgNP formulations to target SSTRs expressed in lungs is also potentially beneficial in the future treatment of other cancers that express SSTRs. The results obtained in targeting the lungs in the present study also corroborated a previous finding that SST analogs coated with AuNPs target SSTR-expressing cancer cells [14]. Other studies also provided details on VAP-coated quantum dots (QDs) and showed that the formulated VAP-QDs can be delivered to BON-1 cells overexpressing $SSTR_2$ [17]. SST has a longer peptide sequence, while OCT has a shorter sequence that is feasible in many ways for conjugation, targeting, and delivery. OCT also selectively binds to $SSTR_2$ [76]. Biomechanical considerations for current targeting by OCT have been proposed, wherein a binding interface has been depicted that exhibits both hydrophobic and hydrophilic interactions between the peptide residues. Ala-Gly-*Cys(cyclo)-Lys-Asn-Phe-Trp-Lys-Thr-Phe-Ser-*Cys-(*cyclo)-OH is the amino acid sequence of $SSTR_2$ that is involved in binding with the Phe-Lys residues of OCT. A preliminary binding model of the interaction between the SSTR and OCT is shown in Figure 1. The pharmacophore-containing residues Phe-Trp-Lys-Thr of the SSTR bind with the incoming ligand to exert its biological activity. A parallel and detailed mechanistic study of the binding interactions is available [77].

The AgNPs–CTT, AgNPs–OCT, and AgNPs–OCT–Alg formulations were inhaled *via* nebulization at a dose for each formulation 1.27 mg/kg. This dose was selected based on the results of *in vitro* cytotoxicity and previously reported results of *in vivo* experiments [12,38,78,79]. All formulations were used in the liquid form to be nebulized and not in dry form, as the dried form of AgNPs has the potential for aggregation and cannot be resuspended. Freeze-drying of AgNPs induces aggregation [80]. The animals successfully inhaled the formulated AgNPs

without experiencing drowsiness or coma. The AgNPs–OCT–Alg was more viscous than the other formulas but was successfully nebulized. To determine the amounts of all AgNPs, the lungs in each group of animals were digested and examined for the inhalation of AgNPs. Upon pulmonary delivery, the AgNPs–CTT accumulated in the lungs due to rapid lymphatic uptake through non-specific binding interactions, while the AgNPs–OCT and AgNPs–OCT–Alg formulations accumulated *via* specific and targeted delivery. The proportion of inhaled AgNPs–OCT–Alg was 0.416 ± 5.7 mg/kg$_{tissue}$, which confirmed the successful active targeting of the lung tissue, while only 0.199 ± 3.21 mg/kg$_{tissue}$ was detected for AgNPs–CTT, indicating nonspecific uptake of Ag$^{+\cdot}$ The lungs showed a higher accumulation of AgNPs–OCT and AgNPs–OCT–Alg due to the expression of SSTRs on the lung cells, which specifically bound to the AgNPs-conjugated OCT [47,81,82]. This form of targeting is active, specific, and selective for lung cancer cells, such as those of non-small cell lung cancer. The AgNPs–OCT–Alg was internalized *via* active targeting, while a parallel report described the internalization of AgNPs into A549 human alveolar cells *via* nonspecific targeting [83].

However, numerous new drugs have shown high levels of cytotoxicity, mainly due to myelosuppression. Indeed, the delivery of cytotoxic agents that can selectively target tumor cells is useful in terms of controlling concentration by way of frequency and quantity. A reduction in peripheral toxicity also improves the therapeutic efficacy of chemotherapeutic agents [8]. Previous studies have reported a number of approaches to targeted drug delivery through specific tags on delivery carriers or at the site, compatible with the double-ended molecular structure. Reubi demonstrated that certain SST analogs labeled with radionuclides (^{111}In, ^{90}Y, ^{177}Lu, and ^{68}Ga) and injected intravenously in mice resulted in reductions in tumor masses [84]. Laznickova *et al.* used materials labeled with radioactive compounds to target SST analogs for diagnostic imaging and the treatment of tumors expressing SSTRs [85]. Moreover, it has also been reported that nanoparticulate formulations provide controlled and sustained drug release in the lung tissue, which supplements reduce the frequency of dosing and complement patient compliance. These approaches of targeted delivery, particularly, delivery to the lungs, further provided impetus to our proposal for the alginate-masked and OCT-mediated site-specific and well-targeted delivery of the lungs mediated by SSTRs.

In conclusion, the functionalized AgNPs were successfully produced using the citrate reduction method, and the synthesized AgNPs–CTT was chemically conjugated with OCT to target SSTRs, particularly, the SSTR$_2$. We developed and evaluated a formulation (AgNPs–OCT–Alg) that was capable of delivery to and internalization in the healthy lung tissues through the nebulization route in the animal model. An array of better prospects exists for the AgNPs–OCT–Alg formulation to serve as a specific, active, site-directed, and on-site method of drug delivery by using the currently presented noninvasive drug delivery method, which is plausible and holds further promise. The prepared AgNPs–OCT–Alg successfully targeted healthy lung tissues *in vivo* in a rat model, and in *in vitro* condition in the model breast cancer cell line, MCF-7, through binding to SSTRs. We analytically confirmed that the AgNPs–CTT was coated with OCT and the alginate wrappings. The presence of OCT in the nanoformulations, AgNPs–OCT and AgNPs–OCT–Alg, assisted in on-site delivery and cell targeting. MCF-7 cells showed specific interactions with the prepared AgNPs–OCT–Alg formulation. Moreover, the AgNPs–OCT and AgNPs–OCT–Alg exhibited higher internalization in the lung tissues due to the facile inhalation strategy and subsequent internalization. The *in vivo* experiments also exhibited high levels of biodistribution and high concentrations of AgNPs in the lung tissue, as confirmed by the presence of Ag$^+$ in ICP-OES analyses of several lung tissue samples obtained from various animal experimental groups treated with different nanoformulations and their varying dose concentrations. Further studies are needed for future lung cancer targeting. Also, more studies of animal lung cancer models are required to reflect the accuracy of active targeting of SSTRs by the AgNPs–OCT–Alg in lung tissues and lung cancer.

Author contributions: Conceptualization: A.A.H.A.; Data curation: A.A.H.A., A.H.A., A.A., O.A.R., and A.M.M.; formal analysis: A.A.H.A., R.A.K., and A.M.M.; funding acquisition: A.A.H.A., A.H.A., and O.A.R.; investigation: A.A.H.A., S.M.S., M.A., O.A.R., and A.M.M; methodology: A.A.H.A., S.M.S., A.M.M., and A.M.M.; project administration: A.A.H.A., A.H.A., A.A., and M.A.; resources: A.A.H.A., A.A., and A.M.M.; software: A.A.H.A., M.A., R.A.K., and A.M.M.; supervision: A.A.H.A., A.A., M.A., and O.A.R.;

validation: A.A.H.A. and R.A.K.; visualization, A.H.A., and A.M.M.; writing–original draft: A.A.H.A., R.A.K., A.A., S.M.S., and A.M.M.; writing–review and editing: A.A.H.A., R.A.K., and A.M.M. All authors have accepted responsibility for the entire content of this manuscript and approved its submission.

Conflict of interest: The authors state no conflict of interest.

References

[1] Alghamdi HI, Alshehri AF, Farhat GN. An overview of mortality & predictors of small-cell and non-small cell lung cancer among Saudi patients. J Epidemiol Glob Health. 2018;7(Suppl 1):S1–6.

[2] Vergnenegre A, Chouaid C. Review of economic analyses of treatment for non-small-cell lung cancer (NSCLC). Expert Rev Pharmacoecon Outcomes Res. 2018;18(5):519–28.

[3] Rosenberg SA, Niglio SA, Jo VY, Goydos JS. Interdigitating dendritic cell sarcoma presenting in the skin: diagnosis and the role of surgical resection, chemotherapy and radiotherapy in management. Rare Tumors. 2014;6(4):5573.

[4] Doroshow JH. Redox modulation of chemotherapy-induced tumor cell killing and normal tissue toxicity. J Natl Cancer Inst. 2006;98(4):223–5.

[5] Garbuzenko OB, Mainelis G, Taratula O, Minko T. Inhalation treatment of lung cancer: the influence of composition, size and shape of nanocarriers on their lung accumulation and retention. Cancer Biol Med. 2014;11(1):44–55.

[6] Cooper A, Potter T, Luker T. Prediction of efficacious inhalation lung doses *via* the use of in silico lung retention quantitative structure-activity relationship models and *in vitro* potency screens. Drug Metab Dispos. 2010;38(12):2218–25.

[7] Alotaibi RM, Rezk HR, Juliana CI, Guure C. Breast cancer mortality in Saudi Arabia: modelling observed and unobserved factors. PLoS One. 2018;13(10):e0206148.

[8] Gupta V, Liu YY. New insights on glucosylceramide synthase in cancer drug resistance and myelosuppression. Biochem Pharmacol (Los Angel). 2013;2:120.

[9] AnnuAhmed, S, Kaur G, Sharma P, Singh S, Ikram S. Evaluation of the antioxidant, antibacterial and anticancer (lung cancer cell line A549) activity of Punica granatum mediated silver nanoparticles. Toxicol Res (Camb). 2018;7(5):923–30.

[10] Burdusel AC, Gherasim O, Grumezescu AM, Mogoantă L, Ficai A, Andronescu E. Biomedical applications of silver nanoparticles: an up-to-date overview. Nanomaterials (Basel). 2018;8(9):681.

[11] Kim JK, Kim HP, Park JD, Ahn K, Kim WY, Gulumian M, et al. Lung retention and particokinetics of silver and gold nanoparticles in rats following subacute inhalation co-exposure. Part Fibre Toxicol. 2021;18(1):5.

[12] Jo MS, Kim JK, Kim Y, Kim HP, Kim HS, Ahn K, et al. Mode of silver clearance following 28-day inhalation exposure to silver nanoparticles determined from lung burden assessment including post-exposure observation periods. Arch Toxicol. 2020;94(3):773–84.

[13] Braakhuis HM, Cassee FR, Fokkens PH, de la Fonteyne LJ, Oomen AG, Krystek P, et al. Identification of the appropriate dose metric for pulmonary inflammation of silver nanoparticles in an inhalation toxicity study. Nanotoxicology. 2016;10(1):63–73.

[14] Abdellatif AA, Zayed G, El-Bakry A, Zaky A, Saleem IY, Tawfeek HM. Novel gold nanoparticles coated with somatostatin as a potential delivery system for targeting somatostatin receptors. Drug Dev Ind Pharm. 2016;42(11):1782–91.

[15] Lehman JM, Hoeksema MD, Staub J, Qian J, Harris B, Callison JC, et al. Somatostatin receptor 2 signaling promotes growth and tumor survival in small-cell lung cancer. Int J Cancer. 2019;144(5):1104–14.

[16] Stumpf C, Kaemmerer D, Neubauer E, Sanger J, Schulz S, Lupp A. Somatostatin and CXCR4 expression patterns in adenocarcinoma and squamous cell carcinoma of the lung relative to small cell lung cancer. J Cancer Res Clin Oncol. 2018;144(10):1921–32.

[17] Abdellatif AAH, Abou-Taleb HA, Abd El Ghany AA, Lutz I, Bouazzaoui A. Targeting of somatostatin receptors expressed in blood cells using quantum dots coated with vapreotide. Saudi Pharm J. 2018;26(8):1162–9.

[18] Abdellatif AAH, Aldalaen SM, Faisal W, Tawfeek HM. Somatostatin receptors as a new active targeting sites for nanoparticles. Saudi Pharm J. 2018;26(7):1051–9.

[19] McMahon KA, Zajicek H, Li WP, Peyton MJ, Minna JD, Hernandez VJ, et al. SRBC/cavin-3 is a caveolin adapter protein that regulates caveolae function. Embo J. 2009;28(8):1001–15.

[20] Nilsson O, Kölby L, Wängberg B, Wigander A, Billig H, William-Olsson L, et al. Comparative studies on the expression of somatostatin receptor subtypes, outcome of octreotide scintigraphy and response to octreotide treatment in patients with carcinoid tumours. Br J Cancer. 1998;77(4):632–7.

[21] Nayak T, Norenberg J, Anderson T, Atcher R. A comparison of high- versus low-linear energy transfer somatostatin receptor targeted radionuclide therapy *in vitro*. Cancer Biother Radiopharm. 2005;20(1):52–7.

[22] Romer I, White TA, Baalousha M, Chipman K, Viant MR, Lead JR. Aggregation and dispersion of silver nanoparticles in exposure media for aquatic toxicity tests. J Chromatogr A. 2011;1218(27):4226–33.

[23] Na DH, Murty SB, Lee KC, Thanoo BC, DeLuca PP. Preparation and stability of poly(ethylene glycol) (PEG)ylated octreotide for application to microsphere delivery. AAPS PharmSciTech. 2003;4(4):E72.

[24] Updegrove TB, Correia JJ, Chen YF, Terry C, Wartell RM. The stoichiometry of the Escherichia coli Hfq protein bound to RNA. Rna-a Publication of the Rna Society. 2011;17(3):489–500.

[25] Rahman A, Kumar S, Bafana A, Dahoumane SA, Jeffryes C. Biosynthetic conversion of Ag(+) to highly stable Ag(0) nanoparticles by wild type and cell wall deficient strains of Chlamydomonas reinhardtii. Molecules. 2019;24(1):98.

[26] Abdellatif AAH, Alturki HNH, Tawfeek HM. Different cellulosic polymers for synthesizing silver nanoparticles with antioxidant and antibacterial activities. Sci Rep. 2021;11(1):84.

[27] Abdellatif AAH, El Hamd MA, Salman KH, Abd-El-Rahim AM, El-Maghrabey M, Tawfeek HM. Integrative physicochemical and HPLC assessment studies for the inclusion of lornoxicam

in buffalo's milk fat globules as a potential carrier delivery system for lipophilic drugs. Microchem J. 2020;152:104321.

[28] Rasheed Z, Rasheed N, Abdulmonem WA, Khan MI. MicroRNA-125b-5p regulates IL-1beta induced inflammatory genes *via* targeting TRAF6-mediated MAPKs and NF-kappaB signaling in human osteoarthritic chondrocytes. Sci Rep. 2019;9(1):6882.

[29] Rasheed Z, Al-Shobaili HA, Rasheed N, Mahmood A, Khan MI. MicroRNA-26a-5p regulates the expression of inducible nitric oxide synthase *via* activation of NF-kappaB pathway in human osteoarthritis chondrocytes. Arch Biochem Biophys. 2016;594:61–7.

[30] Abdellatif AAH, Rasheed Z, Alhowail AH, Alqasoumi A, Alsharidah M, Khan RA, et al. Silver citrate nanoparticles inhibit PMA-induced TNFalpha expression *via* deactivation of NF-kappaB activity in human cancer cell-lines, MCF-7. Int J Nanomedicine. 2020;15:8479–93.

[31] Rasheed Z, Rasheed N, Al-Shaya O. Epigallocatechin-3-O-gallate modulates global microRNA expression in interleukin-1beta-stimulated human osteoarthritis chondrocytes: potential role of EGCG on negative co-regulation of microRNA-140-3p and ADAMTS5. Eur J Nutr. 2018;57(3):917–28.

[32] Pollinger K, Hennig R, Breunig M, Tessmar J, Ohlmann A, Tamm ER, et al. Kidney podocytes as specific targets for cyclo (RGDfC)-modified nanoparticles. Small. 2012;8(21):3368–75.

[33] Hennig R, Pollinger K, Tessmar J, Goepferich A. Multivalent targeting of AT1receptors with angiotensin II-functionalized nanoparticles. J Drug Targeting. 2015;23(7–8):681–9.

[34] Chithrani BD, Ghazani AA, Chan WCW. Determining the size and shape dependence of gold nanoparticle uptake into mammalian cells. Nano Lett. 2006;6(4):662–8.

[35] Elbakry A, Zaky A, Liebkl R, Rachel R, Goepferich A, Breunig M. Layer-by-layer assembled gold nanoparticles for siRNA delivery. Nano Lett. 2009;9(5):2059–64.

[36] Abdellatif AAH, Tawfeek HM. Development and evaluation of fluorescent gold nanoparticles. Drug Dev Ind Pharm. 2018;44(10):1679–84.

[37] Sneddon J, Vincent MD. ICP-OES and ICP-MS for the determination of metals: application to oysters. Analytical Letters. 2008;41(8):1291–303.

[38] Tiwari DK, Jin T, Behari J. Dose-dependent in-vivo toxicity assessment of silver nanoparticle in Wistar rats. Toxicol Mech Methods. 2011;21(1):13–24.

[39] Dufort S, Bianchi A, Henry M, Lux F, Le Duc G, Josserand V, et al. Nebulized gadolinium-based nanoparticles: a theranostic approach for lung tumor imaging and radiosensitization. Small. 2015;11(2):215–21.

[40] Martin AR, Thompson RB, Finlay WH. MRI measurement of regional lung deposition in mice exposed nose-only to nebulized superparamagnetic iron oxide nanoparticles. J Aerosol Med Pulm Drug Deliv. 2008;21(4):335–42.

[41] Lee RF, Pickering WF. Effect of precipitate and complex formation on the determination of silver by atomic-absorption spectroscopy. Talanta. 1971;18(11):1083–94.

[42] Yuan JJ, Xie YZ, Han C, Sun W, Zhang K, Zhao J, et al. Determination of trace element silver in animal serum, tissues and organs by microwave digestion-ICP-MS. Guang Pu Xue Yu Guang Pu Fen Xi. 2014;34(9):2533–7.

[43] Helal OK, Mousa AM, Kandeel N. Effect of antox on hippocampal structure in male albino rats exposed to lead toxicity. Egyptian J Histol. 2011;34(4):808–17.

[44] Alshora D, Ibrahim M, Elzayat E, Almeanazel OT, Alanazi F. Defining the process parameters affecting the fabrication of rosuvastatin calcium nanoparticles by planetary ball mill. Int J Nanomed. 2019;14:4625–36.

[45] Abdellatif AAH, Hennig R, Pollinger K, Tawfeek HM, Bouazzaoui A, Goepferich A. Fluorescent nanoparticles coated with a somatostatin analogue target blood monocyte for efficient leukaemia treatment. Pharm Res. 2020;37(11):217.

[46] Sato I, Umemura M, Mitsudo K, Fukumura H, Kim JH, Hoshino Y, et al. Simultaneous hyperthermia-chemotherapy with controlled drug delivery using single-drug nanoparticles. Sci Rep. 2016;6:24629.

[47] Zahr AS, Davis CA, Pishko MV. Macrophage uptake of core-shell nanoparticles surface modified with poly(ethylene glycol). Langmuir. 2006;22(19):8178–85.

[48] Afshinnia K, Baalousha M. Effect of phosphate buffer on aggregation kinetics of citrate-coated silver nanoparticles induced by monovalent and divalent electrolytes. Sci Total Environ. 2017;581–582:268–76.

[49] Khan Z, Al-Thabaiti SA, Obaid AY, Al-Youbi AO. Preparation and characterization of silver nanoparticles by chemical reduction method. Colloids Surf B Biointerfaces. 2011;82(2):513–7.

[50] Li HY, Zhang F. Preparation of spray-dried nanoparticles for efficient drug delivery to the lungs. Methods Mol Biol. 2020;2118:139–45.

[51] Ullrich SJ, Freedman-Weiss M, Ahle S, Mandl HK, Piotrowski-Daspit AS, Roberts K, et al. Nanoparticles for delivery of agents to fetal lungs. Acta Biomater. 2021;123:346–53.

[52] Lokugamage MP, Vanover D, Beyersdorf J, Hatit MZC, Rotolo L, Echeverri ES, et al. Optimization of lipid nanoparticles for the delivery of nebulized therapeutic mRNA to the lungs. Nat Biomed Eng. 2021;5(9):1059–68.

[53] Detsri E, Kamhom K, Ruen-ngam D. Layer-by-layer deposition of green synthesised silver nanoparticles on polyester air filters and its antimicrobial activity. J Exp Nanosci. 2016;11(12):930–9.

[54] Ali ME, Lamprecht A. Spray freeze drying for dry powder inhalation of nanoparticles. Eur J Pharm Biopharm. 2014;87(3):510–7.

[55] Abdellatif AAH. Identification of somatostatin receptors using labeled PEGylated octreotide, as an active internalization. Drug Dev Ind Pharm. 2019;45(10):1707–15.

[56] Salvioni L, Galbiati E, Collico V, Alessio G, Avvakumova S, Corsi F, et al. Negatively charged silver nanoparticles with potent antibacterial activity and reduced toxicity for pharmaceutical preparations. Int J Nanomedicine. 2017;12:2517–30.

[57] Lu GW, Gao P. Emulsions and microemulsions for topical and transdermal drug delivery. In: Handbook of Non-Invasive Drug Delivery Systems. The Netherlands: Elsevier; 2010. p. 59–94.

[58] Ranoszek-Soliwoda K, Tomaszewska E, Socha E, Krzyczmonik P, Ignaczak A, Orlowski P, et al. The role of tannic acid and sodium citrate in the synthesis of silver nanoparticles. J Nanopart Res. 2017;19(8):273.

[59] Abdellatif A. Octreotide labelled fluorescein isothiocyanate for identification of somatostatin receptor subtype 2. Biochem Physiol. 2015;4(183):2.

[60] Fernandes JC, Wang H, Jreyssaty C, Benderdour M, Lavigne P, Qiu X, et al. Bone-protective effects of nonviral gene therapy with folate-chitosan DNA nanoparticle containing interleukin-1

receptor antagonist gene in rats with adjuvant-induced arthritis. Mol Ther. 2008;16(7):1243–51.

[61] Wang XH, Hong X, Zhu L, Wang YT, Bao JP, Liu L, et al. Tumor necrosis factor alpha promotes the proliferation of human nucleus pulposus cells *via* nuclear factor-kappaB, c-Jun N-terminal kinase, and p38 mitogen-activated protein kinase. Exp Biol Med (Maywood). 2015;240(4):411–7.

[62] Xu Y, Wang L, Bai R, Zhang T, Chen C. Silver nanoparticles impede phorbol myristate acetate-induced monocyte-macrophage differentiation and autophagy. Nanoscale. 2015;7(38):16100–9.

[63] Abdellatif A. Targeting of somatostatin receptors using quantum dots nanoparticles decorated with octreotide. J Nanomed Nanotechnol S. 2015;6:2.

[64] Abdellatif AAH, Rasoul SAEl, Osman S. Gold nanoparticles decorated with octreotide for somatostatin receptors targeting. J Pharm Sci & Res. 2015;7(1):14–20.

[65] Shirshahi V, Shamsipour F, Zarnani AH, Verdi J, Saber R. Active targeting of HER2-positive breast cancer cells by Herceptin-functionalized organically modified silica nanoparticles. Cancer Nanotechnol. 2013;4(1–3):27–37.

[66] Terlević R, Perić Balja M, Tomas D, Skenderi F, Krušlin B, Vranic S, et al. Somatostatin receptor SSTR2A and SSTR5 expression in neuroendocrine breast cancer. Ann Diagn Pathol. 2019;38:62–6.

[67] Kumar U, Grigorakis SI, Watt HL, Sasi R, Snell L, Watson P, et al. Somatostatin receptors in primary human breast cancer: quantitative analysis of mRNA for subtypes 1–5 and correlation with receptor protein expression and tumor pathology. Breast Cancer Res Treat. 2005;92(2):175–86.

[68] Li L, Di X, Wu M, Sun Z, Zhong L, Wang Y, et al. Targeting tumor highly-expressed LAT1 transporter with amino acid-modified nanoparticles: toward a novel active targeting strategy in breast cancer therapy. Nanomedicine. 2017;13(3):987–98.

[69] Bhunchu S, Rojsitthisak P. Biopolymeric alginate-chitosan nanoparticles as drug delivery carriers for cancer therapy. Pharmazie. 2014;69(8):563–70.

[70] Panyam J, Labhasetwar V. Biodegradable nanoparticles for drug and gene delivery to cells and tissue. Adv Drug Deliv Rev. 2003;55(3):329–47.

[71] Brown JS. Deposition of particles. In: Comparative biology of the normal lung. The Netherlands: Elsevier; 2015. p. 513–36.

[72] Han SG, Lee JS, Ahn K, Kim YS, Kim JK, Lee JH, et al. Size-dependent clearance of gold nanoparticles from lungs of Sprague-Dawley rats after short-term inhalation exposure. Arch Toxicol. 2015;89(7):1083–94.

[73] Morfeld P, Treumann S, Ma-Hock L, Bruch J, Landsiedel R. Deposition behavior of inhaled nanostructured TiO2 in rats: fractions of particle diameter below 100 nm (nanoscale) and the slicing bias of transmission electron microscopy. Inhal Toxicol. 2012;24(14):939–51.

[74] Lee JH, Kim YS, Song KS, Ryu HR, Sung JH, Park JD, et al. Biopersistence of silver nanoparticles in tissues from Sprague-Dawley rats. Part Fibre Toxicol. 2013;10:36.

[75] Han L, Ravoori M, Wu G, Sakai R, Yan S, Singh S, et al. Somatostatin receptor type 2-based reporter expression after plasmid-based *in vivo* gene delivery to non-small cell lung cancer. Mol Imaging. 2013;12(7):1–10.

[76] Watt HL, Kharmate G, Kumar U. Biology of somatostatin in breast cancer. Mol Cell Endocrinol. 2008;286(1–2):251–61.

[77] Nagarajan SK, Babu S, Sohn H, Madhavan T. Molecular-level understanding of the somatostatin receptor 1 (SSTR1)-ligand binding: a structural biology study based on computational methods. ACS Omega. 2020;5(33):21145–61.

[78] Jasim R, Schneider EK, Han M, Azad MAK, Hussein M, Nowell C, et al. A fresh shine oncystic fibrosis inhalation therapy: antimicrobial synergy of polymyxin B in combination with silver nanoparticles. J Biomed Nanotechnol. 2017;13(4):447–57.

[79] Seiffert J, Buckley A, Leo B, Martin NG, Zhu J, Dai R, et al. Pulmonary effects of inhalation of spark-generated silver nanoparticles in Brown-Norway and Sprague-Dawley rats. Respir Res. 2016;17(1):85.

[80] Abdelwahed W, Degobert G, Stainmesse S, Fessi H. Freeze-drying of nanoparticles: formulation, process and storage considerations. Adv Drug Deliv Rev. 2006;58(15):1688–713.

[81] Lapa C, Hänscheid H, Wild V, Pelzer T, Schirbel A, Werner RA, et al. Somatostatin receptor expression in small cell lung cancer as a prognostic marker and a target for peptide receptor radionuclide therapy. Oncotarget. 2016;7(15):20033–40.

[82] Kanakis G, Grimelius L, Spathis A, Tringidou R, Rassidakis GZ, Öberg K, et al. Expression of somatostatin receptors 1–5 and dopamine receptor 2 in lung carcinoids: implications for a therapeutic role. Neuroendocrinology. 2015;101(3):211–22.

[83] Foldbjerg R, Dang DA, Autrup H. Cytotoxicity and genotoxicity of silver nanoparticles in the human lung cancer cell line, A549. Arch Toxicol. 2011;85(7):743–50.

[84] Reubi JC. Peptide receptors as molecular targets for cancer diagnosis and therapy. Endocr Rev. 2003;24(4):389–427.

[85] Petrik M, Laznickova A, Laznicek M, Zalutsky MR. Radiolabelling of glucose-Tyr3-octreotate with 125I and analysis of its metabolism in rats: comparison with radiolabelled DOTA-Tyr3-octreotate. Anticancer Res. 2007;27(6B):3941–6.